Formation of high-Sn content polycrystalline GeSn films by pulsed laser annealing on co-sputtered amorphous GeSn on Ge substrate*

Lu Zhang(张璐), Hai-Yang Hong(洪海洋), Yi-Sen Wang(王一森), Cheng Li(李成)†,
Guang-Yang Lin(林光杨), Song-Yan Chen(陈松岩), Wei Huang(黄巍), and Jian-Yuan Wang(汪建元)

Department of Physics, OSED, Semiconductor Photonics Research Center, Xiamen University, Xiamen 361005, *China*

(Received 28 June 2017; revised manuscript received 29 July 2017; published online 30 September 2017)

Polycrystalline $Ge_{1-x}Sn_x$ (poly-$Ge_{1-x}Sn_x$) alloy thin films with high Sn content (> 10%) were fabricated by co-sputtering amorphous GeSn (a-GeSn) on Ge (100) wafers and subsequently pulsed laser annealing with laser energy density in the range of 250 mJ/cm^2 to 550 mJ/cm^2. High quality poly-crystal $Ge_{0.90}Sn_{0.10}$ and $Ge_{0.82}Sn_{0.18}$ films with average grain sizes of 94 nm and 54 nm were obtained, respectively. Sn segregation at the grain boundaries makes Sn content in the poly-GeSn alloys slightly less than that in the corresponding primary a-GeSn. The crystalline grain size is reduced with the increase of the laser energy density or higher Sn content in the primary a-GeSn films due to the booming of nucleation numbers. The Raman peak shift of Ge–Ge mode in the poly crystalline GeSn can be attributed to Sn substitution, strain, and disorder. The dependence of Raman peak shift of the Ge–Ge mode caused by strain and disorder in GeSn films on full-width at half-maximum (FWHM) is well quantified by a linear relationship, which provides an effective method to evaluate the quality of poly-$Ge_{1-x}Sn_x$ by Raman spectra.

Keywords: polycrystalline GeSn, high-Sn content, pulsed laser annealing, disorder

PACS: 68.55.ag, 61.66.Dk, 81.15.Fg, 74.62.En **DOI:** 10.1088/1674-1056/26/11/116802

1. Introduction

$Ge_{1-x}Sn_x$ alloys with Sn content higher than about 0.1 are revealed to achieve the transition from indirect to direct band gap.[1–3] Therefore, single crystalline $Ge_{1-x}Sn_x$ have been intensively studied[4,5] as promising materials for light emitting devices[6,7] based fully on group IV elements. In addition, GeSn lasers have been reported[8–10] as the solution to the problem of a lack of monolithic Si-based laser sources. With high carrier mobility exceeding 500 cm^2/(V·s),[11] GeSn can be used for high performance complementary metal-oxide-semiconductor (CMOS) devices.[11–13] All of the above need high-quality single crystalline $Ge_{1-x}Sn_x$ which must meet strict growth conditions. On the other hand, relatively few studies of poly-GeSn which have significant potential for the use in thin film transistors (TFTs) and infrared focal plane array (IRFPA) detectors have been reported.[14,15] Furthermore, the characterization and analysis of disorder in poly-GeSn have scarcely been reported. Therefore, the processing and analysis techniques of poly-GeSn films with large grain size and high Sn content have important values.

High-Sn content poly-GeSn reveals lower crystallization temperature below 400 °C[16,17] and thermal conductivity about 5–9 W·m^{-1}·K^{-1},[17] which is a suitable channel material for high-performance TFTs rather than poly-Si. It even potentially provides a material platform for better performance flexible TFTs. However, the low solid solubility of α-Sn in Ge below 1 at.%[18,19] hinders the development of high-Sn content GeSn. In order to overcome this problem, non-equilibrium techniques such as pulsed laser annealing (PLA) have been extensively used.[20,21] The PLA process provides a local and rapid annealing source and then cools down in an ultra-short time scale of nanoseconds, which is much shorter as compared to rapid thermal annealing (RTA). Besides, PLA can confine the thermally affected zone in the vicinity of the laser treated area. Thus, high crystallinity and high Sn content GeSn can be achieved by PLA.

In this work, we deposit a-GeSn on p-type Ge (100) wafer with 0.088 Ω·cm resistivity by magnetron sputtering and then transform it into poly-GeSn with large grain size (50–94 nm) and high Sn content (10%–18%) using PLA. The GeSn grain size is found to be reduced with the increase of the laser energy density or higher Sn content in the initial a-GeSn. Disorder of poly-crystal GeSn alloys, besides Sn content and strain, has a great impact on the Raman peak shift of Ge–Ge mode. The influence of the energy density of PLA and the Sn content in the initial a-GeSn on the properties of the poly-crystal GeSn is discussed in detail.

2. Experimental procedure

The processes of sample preparation are schematically shown in Fig. 1. After cleaning, the Ge wafer was pre-heated to 450 °C for 30 min at a base pressure about 9×10^{-5} Pa

*Project supported by the National Natural Science Foundation of China (Grant No. 61474094) and the National Basic Research Program of China (Grant No. 2013CB632103).

†Corresponding author. E-mail: lich@xmu.edu.cn

© 2017 Chinese Physical Society and IOP Publishing Ltd

to remove the native germanium oxide. Afterwards, a 50 nm Ge-buffer was first deposited by RF magnetron sputtering with 0.8 Pa pressure using argon. The Ge-buffer layer could effectively cover the surface of the Ge substrate that might contain residual germanium oxide or defects to provide a clean substrate for GeSn film deposition. On the other hand, during PLA annealing, Ge-buffer would crystallize first to polycrystalline with plenty of grain bounds to release a large part of strain in the GeSn film that is induced by the lattice constant and thermal expansion coefficient difference between Ge and GeSn. Then the wafer was cooled to 180 °C for a-$Ge_{1-x}Sn_x$ growth with thickness about 400 nm by RF and DC magnetron co-sputtering. Two a-$Ge_{1-x}Sn_x$ samples with Sn chemical content x of 0.15 and 0.2 were deposited by maintaining a constant RF power of 100 W for the Ge target, while adjusting the DC power of 12 W and 16 W for the Sn target, respectively. For comparison, an a-Ge sample was prepared using the same experimental conditions without Sn element. A 248 nm KrF excimer laser with a pulse duration of 25 ns with the energy density varying from 250 mJ/cm^2 to 550 mJ/cm^2 irradiated the a-Ge and a-GeSn films in nitrogen atmosphere. The beam size was 4 mm×5 mm and the repetition rate was 1 Hz. The relative moving speeds between the sample and the laser beam were fixed at 4 mm/s and 5 mm/s in two perpendicular directions by a moving stage.

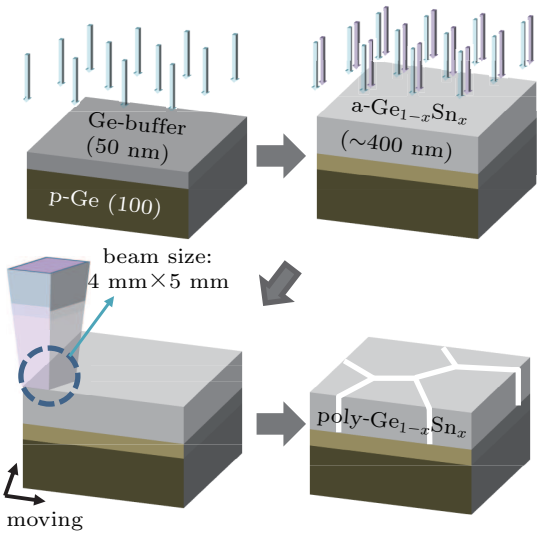


Fig. 1. (color online) Fabrication scheme of poly-GeSn films.

The crystalline phase and Sn content in the samples were characterized by x-ray diffraction (XRD) patterns and selected-area electron diffraction (SAED) patterns. The depth analysis of chemical composition of poly-GeSn by Auger electron spectroscopy (AES) illuminated that the Sn segregation is neither on the surface nor at the interface between the poly-GeSn and buffer-Ge but at the grain boundaries. Transmission electron microscopy (TEM) was used for structural characterization. After etching off the segregated Sn by HCl solution for 3 min, the poly-GeSn grains were visibly observed by scanning electron microscopy (SEM). Additionally, disorder in poly-GeSn which lost long-range orders was analyzed by Raman scattering spectroscopy (spot size: 4 μm, wavelength: 532 nm).

3. Results and discussion

Figure 2 shows the XRD patterns of poly-GeSn films fabricated from a-$Ge_{0.85}Sn_{0.15}$ and a-$Ge_{0.8}Sn_{0.2}$ after PLA with energy density of 250 mJ/cm^2, 400 mJ/cm^2, and 550 mJ/cm^2, respectively. The diffraction peaks of GeSn (111) and (220) are observed obviously in samples a-$Ge_{0.85}Sn_{0.15}$ and a-$Ge_{0.8}Sn_{0.2}$ after the PLA process at energy density from 250 mJ/cm^2 to 550 mJ/cm^2, while the diffraction peak of GeSn (311) is difficult to be distinguished from the adjacent background peaks. The peaks become narrower with increasing laser energy density from 250 mJ/cm^2 to 400 mJ/cm^2, but wider with further increasing laser energy density to 550 mJ/cm^2. Simultaneously, the diffraction peak of β-Sn (101) appears in the samples after PLA at energy density of 400 mJ/cm^2 and 550 mJ/cm^2, suggesting that serious Sn segregation occurs during the crystallization of GeSn. Even more, the irradiated regions by laser with 550 mJ/cm^2 show obvious black traces and the surface becomes rougher. The highest crystallinity after PLA is obtained at an energy density below the occurrence of damage about 550 mJ/cm^2. The substitutional Sn concentration in poly-GeSn films is estimated from the GeSn (111) and (220) peak positions in the XRD patterns using Vegard's law

$$a_0^{Ge_{1-x}Snx} = a_0^{Ge}(1-x) + a_0^{Sn}x, \tag{1}$$

where a_0 is the lattice constant and x is the Sn content. Ge-buffer would release a large part of the strain in the GeSn film that is induced by the lattice constant and thermal expansion coefficient difference between Ge and GeSn. In addition, the strain would release at the poly-GeSn grain boundaries. Therefore, we mainly consider the effect of Sn alloying on the lattice constant. The GeSn (111) peak of the sample a-$Ge_{0.85}Sn_{0.15}$ after PLA with 250 mJ/cm^2 at 2θ of 26.90° is detected at lower angles compared with the Ge (111) peak at 2θ of 27.32°. The lattice constant of GeSn is calculated to be 0.5736 nm using Bragg's law. The Sn content is calculated to be 10.2% using Eq. (1). In the same way, the Sn content x for the poly-$Ge_{1-x}Sn_x$ films fabricated from samples of a-$Ge_{0.85}Sn_{0.15}$ and a-$Ge_{0.8}Sn_{0.2}$ after PLA are calculated and tabulated in Table 1. We discover that the laser energy density of 400 mJ/cm^2 is the optimized choice, with which high crystal quality and high-Sn content poly-GeSn can be obtained.

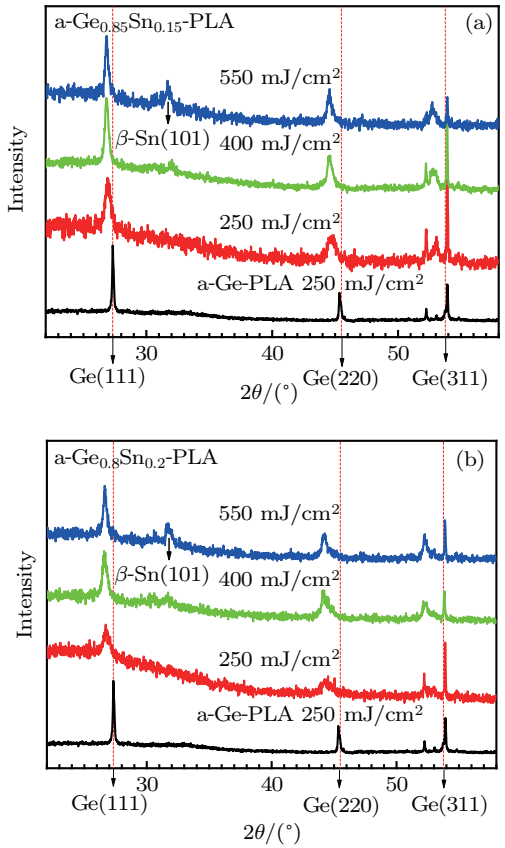


Fig. 2. (color online) XRD patterns of poly-Ge and poly-GeSn films fabricated from (a) a-$Ge_{0.85}Sn_{0.15}$ and (b) a-$Ge_{0.8}Sn_{0.2}$ after PLA with energy density of 250 mJ/cm^2, 400 mJ/cm^2, and 550 mJ/cm^2.

Table 1. Sn contents for poly-$Ge_{1-x}Sn_x$ films fabricated from samples a-$Ge_{0.85}Sn_{0.15}$ and -$Ge_{0.8}Sn_{0.2}$ after PLA. The values x_1, and x_2 are calculated from the diffraction peaks of GeSn (111) and (220) in the XRD patterns, respectively.

Laser energy density/mJ·cm^{-2}	a-$Ge_{0.85}Sn_{0.15}$-PLA x_1, x_2/%	a-$Ge_{0.8}Sn_{0.2}$-PLA x_1, x_2/%
250	10.2, 10.6	14.9, 15.2
400	11.6, 13.9	17.6, 18.2
550	11.2, 13.2	16.3, 17.9

In order to analyze the disorder in the polycrystalline films by Raman scattering spectroscopy, we have prepared poly-Ge films on Ge (100) wafers with different crystalline qualities using PLA with 250 mJ/cm^2 and RTA at 600 °C. Figure 3(a) shows the Raman scattering spectroscopy of bulk Ge (red line), as-deposited a-Ge (black line), poly-Ge crystallized by PLA with 250 mJ/cm^2 (green line), and RTA at 600 °C (blue line). Because the deposited films and the substrates are the same material Ge, the Ge–Ge mode peak shift compared to that of bulk Ge is considered to be mainly induced by the disorder, rather than strain, in the polycrystalline material. Furthermore, the disorder is always associated with peak broadening in Raman scattering spectroscopy. The data of the Raman shift of the Ge–Ge peak and the full width at half maximum (FWHM) are plotted in Fig. 3(d). Narrower FWHM of poly-Ge which illustrates higher crystallinity is attained by using PLA rather than RTA, which is in good agreement with the results extracted from the XRD patterns (not shown here).

Figures 3(b) and 3(c) show Raman spectra of the poly-$Ge_{1-x}Sn_x$ films with different Sn contents after PLA at energy density of 250 mJ/cm^2, 400 mJ/cm^2, and 550 mJ/cm^2, respectively. The Raman shift of the Ge–Ge peak can be attributed to Sn substitution of Ge into the lattice and in-plane strain as well as the disorder influence. The peak shift ($\Delta\omega = \omega_{\mathrm{GeSn}} - \omega_{\mathrm{Ge}}$) compared to the Ge–Ge Raman peak from bulk Ge can be expressed as

$$\Delta\omega = \Delta\omega_{\mathrm{alloy}} + \Delta\omega_{\mathrm{strain+disorder}}, \tag{2}$$

where $\Delta\omega_{\mathrm{alloy}} = ax$ is induced by substitutional Sn content x with coefficient $a = -(82 \pm 4)$,[22] $\Delta\omega_{\mathrm{strain+disorder}}$ is defined as a Raman shift induced by minimal residual amounts of strain and the disorder of GeSn. With the Sn content x in the poly-$Ge_{1-x}Sn_x$ extracted from the XRD patterns, the dependence of the Ge–Ge mode peak shift $\Delta\omega_{\mathrm{strain+disorder}}$ in a-Ge and poly-$Ge_{1-x}Sn_x$ ($0 \le x \le 0.18$) on FWHM is calculated and plotted in Fig. 3(d). The relationship between $\Delta\omega_{\mathrm{strain+disorder}}$ and FWHM (Γ) can be well fitted with a linear relationship

$$\Delta\omega_{\mathrm{strain+disorder}} = -(0.6\Gamma - 3.2) \pm 0.3. \tag{3}$$

This linear relationship provides a non-destructive measurement for conveniently evaluating the quality of poly-GeSn with Raman spectroscopy. Furthermore, Raman shift $\Delta\omega_{\mathrm{strain+disorder}}$ of the poly-$Ge_{1-x}Sn_x$ films which have the highest crystallinity of poly-GeSn using PLA with 400 mJ/cm^2 is shown in Fig. 3(e).

The depth distribution of chemical elements in the poly-$Ge_{0.85}Sn_{0.15}$ film formed by PLA on a-$Ge_{0.8}Sn_{0.2}$ at 250 mJ/cm^2 was measured by AES and shown in Fig. 4(a). The films were argon ion etched to the depth for analysis with an etching rate of about 23 nm/min. As a result, the substitutional Sn concentration in poly-GeSn was slightly lower than the chemical Sn concentration. The result demonstrates that the Sn profile in depth is uniform and Sn segregation occurs at the grain boundaries rather than on the surface or at the interface between the poly-GeSn and buffer-Ge. Figure 4(b) shows the TEM image of the sample of poly-$Ge_{0.85}Sn_{0.15}$. Clear lattice fringes in the high-resolution TEM images indicate high-oriented poly-GeSn with high crystallinity. The SAED patterns of poly-$Ge_{0.85}Sn_{0.15}$ shown in Fig. 4(c) reveal the polycrystalline structure. Bright spots on the 111 ring of GeSn crystals indicate it is highly (111) textured. Sn contents of poly-$Ge_{1-x}Sn_x$ calculated from 111, 220, and 311 halo rings of GeSn crystals are 16.1%, 12.2%, and 15.2%, respectively. The results are broadly in line with the data in Table 1. The difference of Sn contents for different orientations might stem from instrument measuring error, calculation error, or the inhomogeneity of the sample.

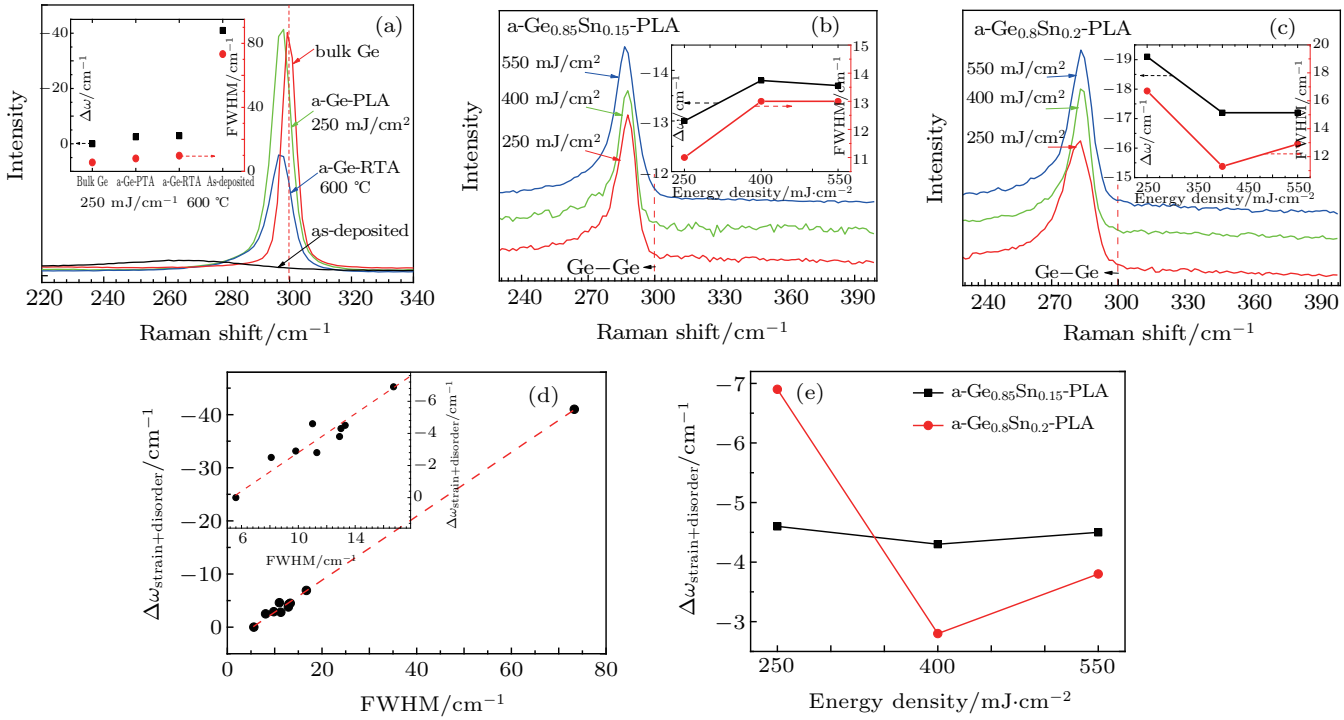


Fig. 3. (color online) Raman scattering spectroscopy of samples: (a) as-deposited a-Ge and poly-Ge crystallized by PLA with 250 mJ/cm^2 and RTA at 600 ^{o}C, (b) a-$Ge_{0.85}Sn_{0.15}$ and (c) a-$Ge_{0.8}Sn_{0.2}$ after the PLA process at energy density of 250 mJ/cm^2, 400 mJ/cm^2, and 550 mJ/cm^2. The insets show trends of FWHM and $\Delta\omega$ respected to (a) different crystalline qualities and (b), (c) different energy density. (d) The Ge–Ge mode peak shift $\Delta\omega_{\text{strain+disorder}}$ in a-Ge and poly-$Ge_{1-x}Sn_x$ ($0 \le x \le 0.18$) caused by strain and disorder depends on FWHM. The dash line is a linear fit to the data. The inset zooms into the data of poly-$Ge_{1-x}Sn_x$ ($0 \le x \le 0.18$). (e) The Ge–Ge mode peak shift $\Delta\omega_{\text{strain+disorder}}$ in poly-GeSn films fabricated from a-$Ge_{0.85}Sn_{0.15}$ and a-$Ge_{0.8}Sn_{0.2}$ after PLA with energy density of 250 mJ/cm^2, 400 mJ/cm^2, and 550 mJ/cm^2.

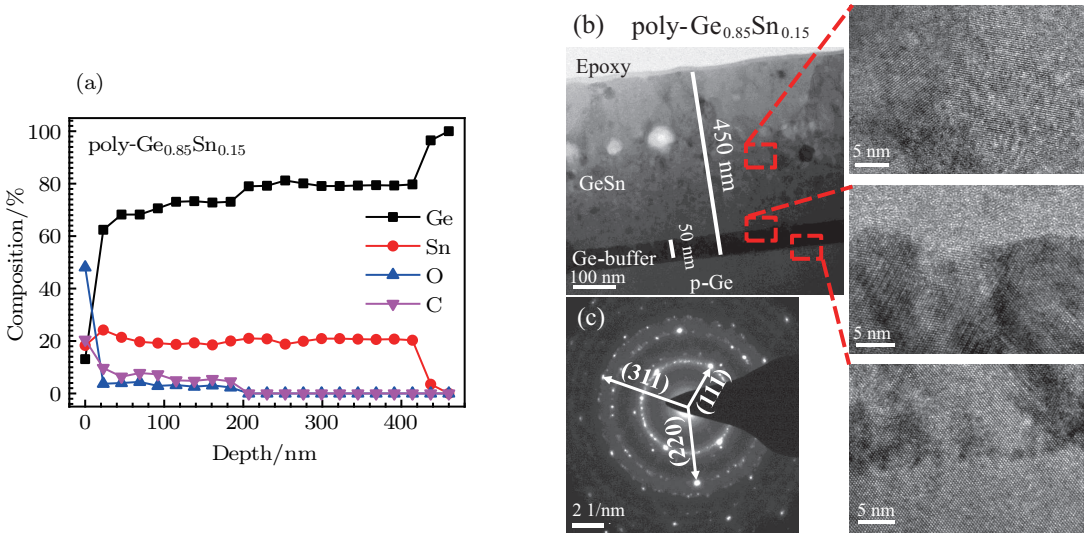


Fig. 4. (color online) (a) AES scan, (b) TEM image, (c) and SAED patterns of the sample poly-$Ge_{0.85}Sn_{0.15}$.

After etching off the segregated Sn at the grain boundaries by HCl solution for 3 min, the poly-GeSn grains were visibly observed in SEM images as shown in Fig. 5. The average grain size of poly-GeSn becomes smaller with the increase of the laser energy density or higher Sn content in the primary a-GeSn films. With higher laser energy, enhancing nucleation results in the reduction of the crystalline grain size. The crystallization temperature of GeSn alloy decreases with increasing Sn content and therefore the poly-GeSn grain size reduces as well. High quality poly-crystal $Ge_{0.90}Sn_{0.1}$ and $Ge_{0.82}Sn_{0.18}$ films with average grain sizes of 94 nm and 54 nm were attained, respectively.

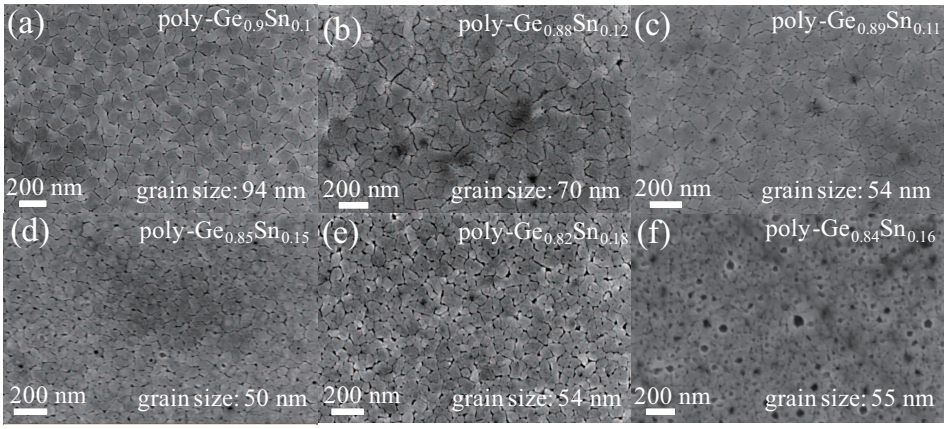


Fig. 5. SEM images of poly-GeSn films fabricated from (a)–(c) a-$Ge_{0.85}Sn_{0.15}$ and (d)–(f) a-$Ge_{0.8}Sn_{0.2}$ after PLA with energy density of 250 mJ/cm^2, 400 mJ/cm^2, and 550 mJ/cm^2, respectively.

4. Conclusion

We demonstrated the growth of poly-$Ge_{1-x}Sn_x$ films with high Sn content (10%–18%) on Ge substrates using pulsed laser annealing on co-sputtered a-GeSn. It is shown that the crystalline grain size of poly-GeSn decreases with the increase of the laser energy density or Sn content in the primary a-GeSn film, both of which enhance the nucleation of a-GeSn. High crystal quality $Ge_{0.90}Sn_{0.1}$ and $Ge_{0.82}Sn_{0.18}$ films with average grain sizes of 94 nm and 54 nm were grown. The uniform distribution of Sn element in depth and SEM images of the etched poly-GeSn films show that Sn segregation occurs at the grain boundaries rather than on the surface or at the interface between the poly-GeSn and buffer-Ge. The dependence of Ge–Ge mode peak shift caused by strain and disorder on FWHM is well quantified by a linear relationship, which commendably provides an effective method to evaluate the quality of poly-$Ge_{1-x}Sn_x$ by Raman spectra. As poly-Ge can be used for multiple flexible devices such as metal–semiconductor–metal photodiodes,[23] TFTs, and IRFPA,[24] poly-GeSn should be a very promising material to improve the performance of the above devices for the electrical properties enhanced by the doping of Sn into Ge. Hence, further study on high quality GeSn is necessary and significant.

References

[1] Peŕez Ladroń de Guevara H, Rodríguez A G, Navarro-Contreras H and Vidal M A 2004 *Appl. Phys. Lett.* **84** 4532
[2] Eckhardt C, Hummer K and Kresse G 2014 *Phys. Rev. B* **89** 165201
[3] Li H F, Wang X X and Liu J F 2016 *Appl. Phys. Lett.* **108** 10210
[4] Bhargava N, Coppinger M, Gupta J P, Wielunski L and Kolodzey J 2013 *Appl. Phys. Lett.* **103** 041908
[5] Su S J, Wang W, Cheng B W, Zhang G Z, Hu W X, Xue C L, Zuo Y H and Wang Q M 2011 *J. Cryst. Growth* **317** 43
[6] Tseng H H, Wu K Y, Li H, Mashanov V, Cheng H H, Sun G and Soref R A 2013 *Appl. Phys. Lett.* **102** 182106
[7] Oehme M, Kostecki K, Arguirov T, Mussler G, Ye K, Gollhofer M, Schmid M, Kaschel M, Körner R A, Kittler M, Buca D, Kasper E and Schulze J 2014 *IEEE Photonics Tech. Lett.* **26** 187
[8] Al-Kabi S, Ghetmiri S A, Margetis J, Pham T, Zhou Y Y, Dou W, Collier B, Quinde R, Du W, Mosleh A, Liu J F, Sun G, Soref R A, Tolle J, Li B H, Mortazavi M, Naseem H A and Yu S Q 2016 *Appl. Phys. Lett.* **109** 171105
[9] Driesch N V D, Stange D, Wirths S, Mussler G, Holländer B, Ikonic Z, Hartmann J M, Stoica T, Mantl S, Grützmacher D and Buca D 2015 *Chem. Mater.* **27** 4693
[10] Stange D, Wirths S, Geiger R, Schulte B C, Marzban B, Driesch N V D, Mussler G, Zabel T, Stoica T, Hartmann J M, Mantl S, Ikonic Z, Grützmacher D, Sigg H, Witzens J and Buca D 2016 *ACS Photonics* **3** 1279
[11] Fang Y C, Chen K Y, Hsieh C H, Su C C and Wu Y H 2015 *ACS Appl. Mater. Inter.* **7** 26374
[12] Gupta S, Simoen E, Loo R, Madia O, Lin D, Merckling C, Shimura Y, Conard T, Lauwaert J, Vrielinck H and Heyns M 2016 *ACS Appl. Mater. Interfaces* **8** 13181
[13] Maeda T, Jevasuwan W, Hattori H, Uchida N, Miura S, Tanaka M, Santos N D M, Vantomme A, Locquet J P and Lieten R R 2015 *J. Appl. Phys.* **54** 04DA07
[14] Kim M, Fan W J, Seo J H, Cho N, Liu S C, Geng D, Liu Y H, Gong S Q, Wang X D, Zhou W D and Ma Z Q 2015 *Appl. Phys. Express* **8** 061301
[15] Kurosawa M, Taoka N, Sakashita M, Nakatsuka O, Miyao M and Zaima S 2013 *Appl. Phys. Lett.* **103** 101904
[16] Zhang L, Wang Y S, Chen N L, Lin G Y, Li C, Huang W, Chen S Y, Xu J F and Wang J Y 2016 *J. Non-Cryst. Solids* **448** 74
[17] Uchida N, Maeda T, Lieten R R, Okajima S, Ohishi Y, Takase R, Ishimaru M and Locquet J P 2015 *Appl. Phys. Lett.* **107** 232105
[18] Thurmond C D, Trumbore F A and Kowalchik M 1956 *J. Chem. Phys.* **25** 799
[19] Mahmodi H and Hashim M R 2017 *Chin. Phys. B* **26** 056801
[20] Moto K, Matsumura R, Sadoh T, Ikenoue H and Miyao M 2016 *Appl. Phys. Lett.* **108** 262105
[21] Stefanov S, Conde J C, Benedetti A, Serra C, Werner J, Oehme M, Schulze J, Buca D, Holländer B, Mantl S and Chiussi S 2012 *Appl. Phys. Lett.* **100** 104101
[22] Lin H, Chen R, Huo Y, Kamins T I and Harris J S 2011 *Appl. Phys. Lett.* **98** 261917
[23] Kim M, Seo J H, Yu Z, Zhou W D and Ma Z Q 2016 *Appl. Phys. Lett.* **109** 051105
[24] Shahrjerdi D, Hekmatshoar B, Mohajerzadeh S S, Khakifirooz A and Robertson M 2004 *J. Electeron. Mater.* **33** 4